# Noise properties of nanoscale $YBa_2Cu_3O_{7-\delta}$ Josephson junctions

D. Gustafsson,* F. Lombardi, and T. Bauch
*Department of Microtechnology and Nanoscience, Chalmers University of Technology, SE-412 96 Göteborg, Sweden*
(Received 29 June 2011; revised manuscript received 5 October 2011; published 28 November 2011)

We present electric noise measurements of nanoscale biepitaxial $YBa_2Cu_3O_{7-\delta}$ (YBCO) Josephson junctions fabricated by two different lithographic methods. The first (conventional) technique defines the junctions directly by ion milling etching through an amorphous carbon mask. The second (soft patterning) method makes use of the phase competition between the superconducting YBCO (Y123) and the insulating $Y_2BaCuO_5$ (Y211) phase at the grain boundary interface on MgO (110) substrates. The voltage noise properties of the two methods are compared in this study. For all junctions (having a thickness of 100 nm and widths of 250–500 nm), we see a significant amount of individual charge traps. We have extracted an approximate value for the effective area of the charge traps from the noise data. From the noise measurements, we infer that the soft-patterned junctions with a grain-boundary (GB) interface manifesting a large *c*-axis tunneling component have a uniform barrier and a superconductor-insulator-superconductor (SIS) -like behavior. The noise properties of soft-patterned junctions having a GB interface dominated by transport parallel to the *ab* planes are in accordance with a resonant tunneling barrier model. The conventionally patterned junctions, instead, have suppressed superconducting transport channels with an area much less than the nominal junction area. These findings are important for the implementation of nanosized Josephson junctions in quantum circuits.

DOI: 10.1103/PhysRevB.84.184526 PACS number(s): 74.72.−h, 74.50.+r

## I. INTRODUCTION

Micrometer-sized grain boundary (GB) Josephson junctions (JJs) made of high-critical-temperature superconductors (HTS) are commonly used for the realization of superconducting devices operated in a wide temperature range up to the boiling temperature of liquid nitrogen. A prominent example is the superconducting quantum interference device (SQUID) for sensitive magnetic flux detection.[1] Nevertheless, GB JJs are still a fundamental tool for the exploration of the complex physics inherent to HTS materials.[2–6] Their implementation in superconducting circuits operated in the quantum limit, such as quantum bits or single-electron transistors, are expected to give further useful hints on the unresolved nature of superconductivity in HTS materials.[7] Recent advances in the thin film technology and nanofabrication of HTS made it possible to observe macroscopic quantum phenomena in $YBa_2Cu_3O_{7-\delta}$ (YBCO) biepitaxial grain boundary Josephson junctions[5,6] opening the way for the realization of HTS quantum circuits. For typical JJ-based devices, which operate in the quantum limit (typically at temperatures below 100 mK), the requirements on junction critical currents and capacitances are met for lateral dimensions on a length scale of 100 nm.[7,8]

The realization of reproducible HTS JJs at the nanoscale can also be instrumental to fabricate sensors with a quantum limited sensitivity like nano-SQUIDs, which can allow the detection of magnetic nanoparticles in a much wider temperature and magnetic field range compared to its low-critical-temperature superconductor (LTS) counterpart.

In this respect, it is of particular importance to understand the microscopic properties and dynamics of charge transport across nanosized GB JJs. Here, the investigation of low-frequency electric noise is a very useful tool to study the dynamics of both cooper pair and quasiparticle charge transport, revealing among other things information about the nature of the GB interface and its homogeneity. Still after numerous experimental studies on HTS GB junctions during the last decades, the underlying physical transport mechanisms across the GB interface are subject of recurring discussion.

A large number of noise studies have been performed on wide bicrystal and biepitaxial GB JJs with junction widths ranging from one to several tens of micrometers.[9–14] Only a few electric transport studies have been performed on submicrometer bicrystal GBs, where single charge trapping states, responsible for the low-frequency fluctuations of the transparency of the GB barrier, could be resolved.[15]

In this paper, we compare two methods to fabricate YBCO Josephson junctions at the nanoscale and their respective noise properties. These methods are based on biepitaxial grain boundaries created in single-layer YBCO films. Both a conventional technique, where the nanosized junctions are patterned by electron beam lithography and ion milling, and a new technique, where the junctions are formed as a result of phase competition between superconducting and insulating phases at the grain boundary interface, will be described. We have previously shown that the two methods give Josephson junctions with fundamentally different critical current density, $j_C$, and resistivity, $\rho_N$, values.[16] In this paper, we compare the noise data of soft nanopatterned GB junctions to various electrical transport models, which allows us to determine the nature of the biepitaxial GB barriers. Moreover, from the analysis of single charge trap states in the GB barriers, we are able to qualitatively and quantitatively assess the detrimental effect of ion milling on GBs during the conventional fabrication.

This paper is organized as follows. In Sec. II, we describe both the conventional and soft nanostructuring of biepitaxial YBCO JJs. Section III is dedicated to the comparison of the dc transport properties between junctions fabricated with the two nanopatterning methods. The noise models applicable to GB JJs are introduced in Sec. IV. In Sec V, we present the results

 

and discussion of noise measurements on JJs fabricated with the two nanolithographic methods.

## II. SAMPLE FABRICATION

### A. Conventional nanostructuring

The conventional way to fabricate deep submicron biepitaxial Josephson junctions is to use electron beam lithography in combination with a hard mask and ion beam milling. This procedure, with amorphous carbon as hard mask, is well established and has been proven to work well for the realization of various kinds of submicron HTS Josephson junctions, for example ramp type,[17] bicrystal,[18] and biepitaxial.[19] In this work, we have fabricatated deep submicron Josephson junctions by the biepitaxial technique. Details on the fabrication procedure can be found elsewhere.[19,20] Here, we only summarize the main steps. First, a 30-nm-thick $SrTiO_3$ (STO) layer is deposited on a MgO (110) substrate using pulsed laser deposition (PLD). Next, an amorphous carbon mask is deposited and then patterned using e-beam lithography and oxygen plasma. Part of the seed layer is then removed using ion milling. Then a 100–120-nm-thick YBCO film is grown by PLD at a temperature of 790 °C. The film will grow (001) oriented on the MgO substrate and (103) on the STO seed layer. The YBCO film is then patterned using ion milling through an amorphous carbon mask defined by e-beam lithography. Even though junctions with widths smaller than 100 nm can, in principle, be fabricated with this procedure, the damage caused by the ion milling process will effectively limit the smallest possible width. The damaged grain-boundary region on both sides of the junction constitutes a significant part of the total junction width, which strongly affects the superconducting properties. We have therefore engineered an alternative way to nanostructure HTS Josephson junctions, which is described in the following section.

### B. Soft nanostructuring

We have developed a soft patterning method that allows fabricating biepitaxial grain boundary junctions at the nanoscale without significant lateral damaging effects due to the ion milling. The procedure is based on the competition between the nucleation of the superconducting and insulating phases at the grain boundary. To fabricate the junctions, we use the fact that for certain deposition conditions, secondary insulating phases like $Y_2BaCuO_5$ (Y211, also called greenphase) can nucleate on MgO(110) in addition to the superconducting $YBa_2Cu_3O_{7-\delta}$ (Y123). The amount of greenphase increases for nonoptimal deposition conditions and in the presence of grain boundaries.[8,21,22] Nanosized superconducting Y123 connections embedded in a greenphase matrix are expected to be formed at the grain boundary, see Fig. 1(a). These connections can be isolated using a focused ion beam (FIB), see Figs. 1(b) and 1(c).

We first fabricate 10-$\mu$m-wide grain-boundary junctions using the conventional method. A deposition temperature of 740 °C is used for the YBCO film. The grain boundary is then examined using atomic force microscopy (AFM) and scanning electron microscopy (SEM). A suitable superconductive nanoconnection is selected and then isolated by using FIB. By leaving greenphase regions of at least 300 nm on each side of the Y123 connection, nanosized Josephson junctions with no lateral damage are created, since the Ga ions will only get implanted into the greenphase layer. Figure 1(c) shows a final device, where we have isolated an approximately 200-nm-wide junction protected on both sides by greenphase.

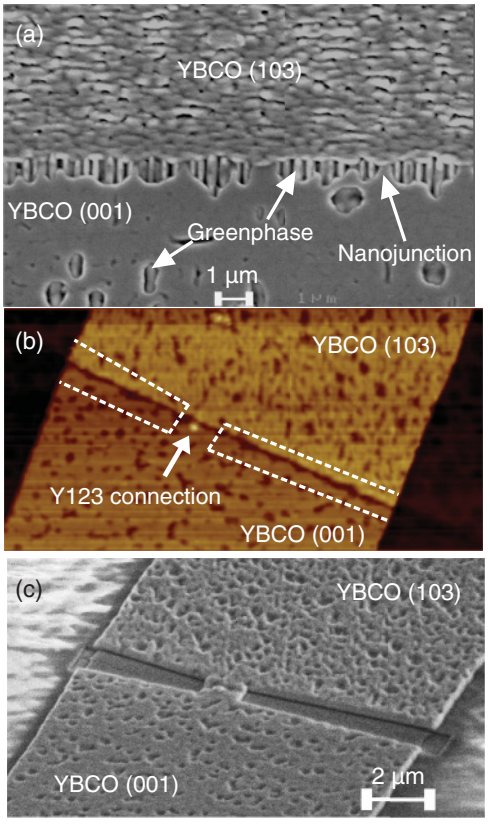


FIG. 1. (Color online) (a) SEM image of an interface between a (001) and (103) YBCO film. A significant amount of greenphase is present near the grain boundary. In a different study,[16] transmission electron microscopy and energy-dispersive x-ray analysis was used to confirm that the precipitate at the grain boundary is greenphase. (b) AFM scan of a 10-$\mu$m-wide grain boundary interface before the FIB procedure. (c) SEM image of the same interface after the unwanted YBCO have been removed by the FIB leaving only one or two connections.

## III. COMPARISON BETWEEN THE TRANSPORT PROPERTIES OF CONVENTIONAL AND SOFT NANOPATTERNED JUNCTIONS

Electrical properties such as critical current density ($j_C$), specific resistance ($\rho_N$), and critical current ($I_C$) versus magnetic field ($B$) have been extensively examined[16] and have shown significant differences for the two fabrication methods. Figure 2 shows the current-voltage characteristics (IVC) for (a) a soft nanopatterned (200-nm-wide), (b) a 300-nm-wide conventionally patterned, and (c) a 200-nm-wide conventionally patterned junctions. A recurring pattern is seen here: the soft-nanostructured junctions have an order of magnitude or more higher $j_C$ and one or several orders of magnitude lower $\rho_N$ when compared to conventionally fabricated samples. Conventionally fabricated junctions with a

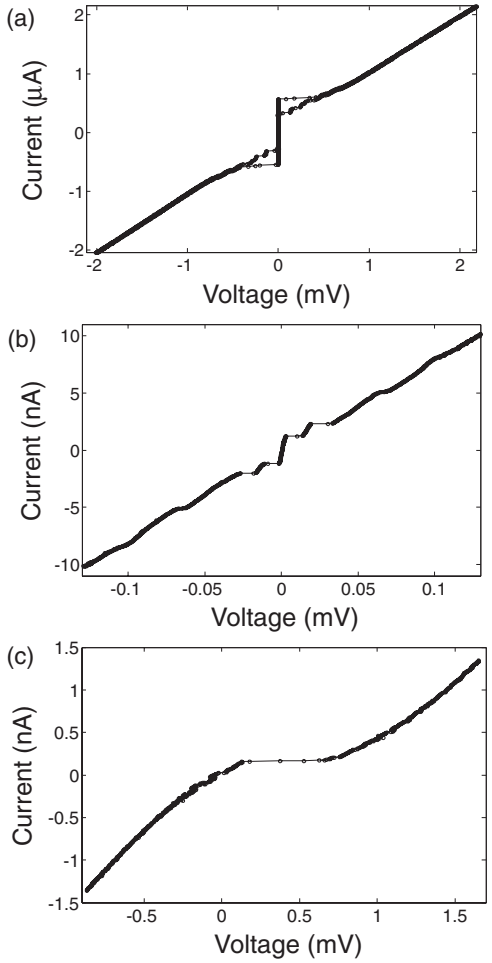


FIG. 2. Current-voltage characteristics for (a) a nanojunction fabricated using the soft-nanopatterning technique. The width of the junction extracted from AFM is 200 nm. (b) Sample fabricated with the conventional nanopatterning technique. The second switch is because this specific sample was designed to have two Josephson junctions in series to allow study of charging effects. Here, the nominal junction width is 300 nm. (c) Sample fabricated using the conventional method, 200 nm wide, with a Coulomb-blockade-like behavior and no critical current. The measurements were done at 271, 16, and 22 mK, respectively.

width of 200 nm or less have high resistive nonlinear IVCs with a suppressed Josephson current. Only junctions with widths 300 nm or more showed a Josephson current.

$I_C$ versus $B$ measurements revealed significant differences in the modulation period for the two fabrication methods. The period of the magnetic-field modulation ($\Delta B$) of the Josephson current can be used to approximate the width ($w$) of the region exhibiting Josephson coupling in the junctions. Figure 3(a) shows the $I_C$ versus $B$ for a 10-$\mu$m-wide grain boundary junction before the FIB cut to isolate the nanojunction; the behavior of the magnetic pattern is that of several parallel junctions.[23,24] Figure 3(b) shows the magnetic pattern of a soft-patterned junction after the FIB cut, leaving only one or two connections.

Depending on the electrode geometry, we use the two expressions for $\Delta$B as a function of the junction width $w_j$ from Rosenthal and coworkers.[25,26] For the soft-patterned

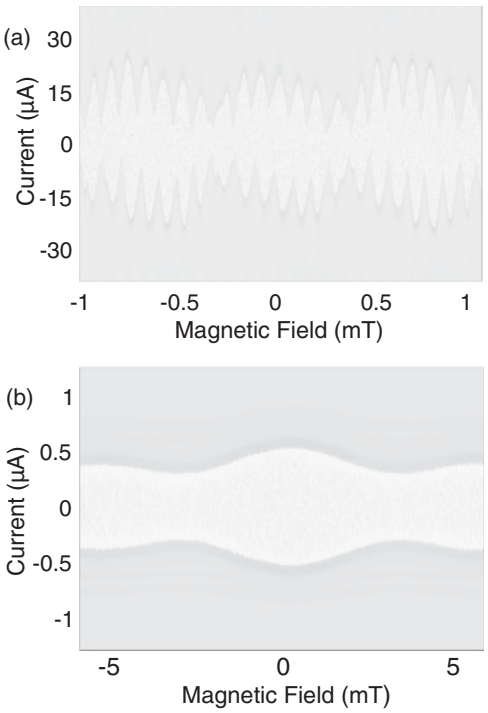


FIG. 3. $I$ vs $B$ for (a) a 10-$\mu$m-wide grain boundary with many parallel channels. (b) Sample cut by FIB, which consists of only one or two parallel channels. The grey scale represents the logarithmic conductance and the darkest region corresponds to $I_C$.

junctions having wide electrodes $w_e \simeq 10\ \mu$m, we use the thick-electrode limit expression

$$\Delta B = \frac{\Phi_0 t}{1.2 w_j^2 (\lambda_{103} + \lambda_{001} + d)} \tag{1}$$

valid for $\lambda_{001,103}^2/t < w_e$. Here, $\lambda_{001}$ and $\lambda_{103}$ are the London penetration depths in the (001) and (103) electrodes, respectively. $\Phi_0$ is the magnetic flux quantum, $t$ is the thickness of the film, and $d$ is the thickness of the junction barrier. For the conventionally nanopatterned junctions, the width of the electrodes is equal to the width of the junctions $w_e \simeq 300$–$500$ nm. Here, the thin-electrode limit ($\lambda_{001,103}^2/t \geqslant w_e$) applies:

$$\Delta B = \frac{1.84 \Phi_0}{w_j^2}. \tag{2}$$

The London penetration depth in the (001) electrode is given by the penetration depth in the $ab$ planes $\lambda_{001} = \lambda_{ab}$. Instead, as a result of the London penetration depth anisotropy in YBCO, $\lambda_{103}$ is given by a combination of $\lambda_{ab}$ and the $c$-axis penetration depth $\lambda_c$, which depends on the grain boundary angle.[4,28]

Equation (1) was used on a number of soft-patterned junctions and the extracted width was compared to the nominal width measured by AFM and SEM.[16] The values were at most differing by 40%; this shows that the width of the superconducting transport channels extracted from the magnetic pattern was very close to the measured junction widths.

For one of the conventionally nanopatterned junction, $\Delta B$ of approximately 1 T was extracted from the magnetic pattern. Using Eq. (2) resulted in a width of 60 nm, significantly less than the nominal junction width of 300 nm. Similar results

where obtained for two other junctions 300- and 500-nm wide. This in combination with the $j_C$ and $\rho_N$ values shows that a substantial part of the grain boundary, approximately 100-nm wide, on each lateral side of the junction does not feature any Josephson coupling.

The magnetic patterns of conventionally nanopatterned junctions have revealed the presence of a highly nonuniform grain boundary, having a much reduced region with Josephson coupling compared to the nominal one. However, this does not give a clear image of the total area that retains the Josephson coupling along the grain boundary. In fact, it only tells us that the largest spacing between superconducting channels is significantly less than the nominal junction width. To estimate the area of both the Cooper pair and quasiparticle transport channels, we analyzed the voltage noise of the junctions caused by single charge traps in the GB barrier, which will be discussed in Sec. V.

## IV. NOISE THEORY FOR GRAIN-BOUNDARY JUNCTIONS

Noise measurements are a helpful tool to extract information about the electrical transport through the junction and hence to obtain information about the nanostructure of the grain boundary interface. In this work, we focused on the low-frequency noise spectra of both the critical current fluctuations $\delta I_C$ and normal resistance fluctuations $\delta R_N$, which are related to the transport mechanisms of the cooper pairs and quasiparticles, respectively.

It is well established that at low frequencies, the critical current and normal resistance fluctuations are governed by bistable charge trapping states in the junction barrier.[29] The trapping of a charge will locally increase the junction barrier making it less transparent. This process can be considered as a reduction of the total junction area $A_j$ by an amount that is proportional to the cross section of the localized charge trap state $A_t$. The fluctuating barrier transparency (or equivalently junction area) results in fluctuations of the critical current $I_C$ and normal resistance $R_N$. Each individual charge trap causes a random telegraph switching (RTS) signal between two states, with respective mean lifetimes $\tau_1$ and $\tau_2$, of both the junction normal resistance and critical current. The corresponding frequency spectrum is given by a Lorentzian:[30]

$$S_R^{\mathrm{RTS}}(f) = \frac{4\left\langle\left(\frac{\delta R_N}{R_N}\right)^2\right\rangle\tau_{\mathrm{eff}}}{1+(2\pi f\tau_{\mathrm{eff}})^2},$$
$$S_I^{\mathrm{RTS}}(f) = \frac{4\left\langle\left(\frac{\delta I_C}{I_C}\right)^2\right\rangle\tau_{\mathrm{eff}}}{1+(2\pi f\tau_{\mathrm{eff}})^2}, \tag{3}$$

where $\tau_{\mathrm{eff}} = (\tau_1^{-1}+\tau_2^{-1})^{-1}$ is the effective lifetime of the underlying RTS signal and $f$ is the frequency. $\langle(\delta R_N/R_N)^2\rangle$ and $\langle(\delta I_C/I_C)^2\rangle$ are the mean-squared relative fluctuations of the normal resistance and critical current caused by the charge trap. For large enough junction areas, many bistable charge trapping states will contribute to the total noise. Assuming a constant distribution of transition rates $1/\tau_{\mathrm{eff}}$, the resulting noise power spectrum will have a $1/f$ shape.

The values of the relative root mean-square (rms) fluctuations $\delta I_C/I_C$ and $\delta R_N/R_N$ can be determined by measuring the voltage noise across the junction at various bias current values. For a Josephson junction having a nonhysteretic current-voltage characteristic, the total voltage fluctuations across the junction at a fixed bias current $I$ are given by[10]

$$S_V(f) = (V-R_dI)^2S_I(f) + V^2S_R(f) + k(V-R_dI)VS_{IR}(f), \tag{4}$$

where $V$ is the dc voltage across the junction, $R_d = \partial V/\partial I$ is the differential resistance, $S_I = |\delta I_C/I_C|^2$, $S_R = |\delta R_N/R_N|^2$, and $S_{IR} = |\delta I_C/I_C||\delta R_N/R_N|$ is the cross spectral density of the fluctuations. Here, it is assumed that $S_I$ and $S_R$ are composed of an ensemble of RTS signals, $S_I^{\mathrm{RTS}}$ and $S_R^{\mathrm{RTS}}$, respectively. The value $k$ represents the correlation between the $\delta I_C$ and $\delta R_N$ fluctuations. One has $k=-2$ and $k=2$ for perfectly antiphase and inphase correlated fluctuations, respectively. For uncorrelated fluctuations, one obtains $k=0$. From Eq. (4), it follows that at bias currents close to the critical current the voltage fluctuations are dominated by critical current fluctuations $S_I$ due to the large differential resistance. For large bias currents, where the differential resistance approaches the asymptotic normal resistance, the voltage noise is governed by resistance fluctuations $S_V = V^2S_R$. The correlation term $S_{IR}$ will only contribute to the voltage noise in the intermediate bias current regime, while it is negligible close to the critical current and for large bias currents.

The values of the relative fluctuations $\delta I_C/I_C$ and $\delta R_N/R_N$ depend on the nature of the junction barrier. Indeed, from the ratio $q = |\delta I_C/I_C|/|\delta R_N/R_N|$ between the relative fluctuations, one can extract information about the homogeneity of the junction barrier as we will discuss on the basis of the following three junction models applicable to grain boundary junctions.

For a homogenous junction barrier, one can assume that the $I_CR_N$ product is a constant, independent of the critical current density $j_c$ and resistivity $\rho_n$. This is, for example, the case for an SIS junction,[23] where cooper pairs and quasiparticles tunnel (directly) through the same parts of the junction. From the constant $I_CR_N$ product, it follows directly that the relative fluctuations of the critical current and normal resistance have the same amplitude and are anticorrelated, $\delta I_C/I_C = -\delta R_N/R_N$, resulting in a ratio $q=1$.

In the intrinsic shunted junction (ISJ) model,[31,32] instead, where the barrier is assumed to be inhomogeneous containing a high density of localized electron-like states, the quasiparticle transport is dominated by resonant tunneling via the localized states. On the contrary, due to Coulomb repulsion Cooper pairs can only tunnel directly through the barrier. Detailed calculations show that the $I_CR_N$ product is not anymore constant, instead, it follows the scaling behavior $I_CR_N \propto (j_c)^p$, where $j_c$ is the critical current density of the junction and $p$ is a constant depending on the position of the localized states. For localized states sitting in the middle of the barrier, the scaling power is $p=0.5$. From this $I_CR_N$ scaling behavior, one obtains for the ratio of the normalized fluctuations $|\delta I_C/I_C|/|\delta R_N/R_N| = q = 1/(1-p)$.[31] Typical experimental values of $q$ range between 2 and 4.[9,11–13]

The channel model proposed by Micklich *et al.*[10] assumes a junction that consists of $N$ parallel channels, where all channels have the same resistance but only one channel

carries a supercurrent. For a large number of channels $N$, the fluctuations in critical current can be much higher than the fluctuations in resistance, giving a high ratio $q$. Since the supercurrent and the quasiparticles have separate channels, no correlation between the critical current and resistance fluctuations is expected.

## V. RESULTS AND DISCUSSION

The voltage noise spectral density was measured using a room-temperature voltage preamplifier with an input noise of 4 $nV/Hz^{1/2}$ followed by a Stanford Research Dynamic Signal analyzer SR785 for a number of bias points. These measurements were done at 4 K for the soft-nanostructured junctions, where the current-voltage characteristic was nonhysteretic. For the conventionally fabricated samples, a temperature of 280 mK was needed to avoid thermal smearing of the IVC (due to the low $I_C$ of these junctions).[10]

All noise measurements on the conventionally patterned samples refer to grain boundaries obtained by patterning the STO seed layer parallel to the [100] direction ($\theta = 0^\circ$) of the MgO substrate[4] (see Fig. 4). The soft-patterned junctions had nominal interface angles ($\theta$) of 30° and 50°. Grain boundaries with a small interface angle $\theta$ have a microstructure close to a basal-plane-like type (45° [010] tilt), see Fig. 4, where the $ab$ planes of the (001) YBCO electrode meet one single $ab$ plane on the (103) YBCO electrode side.[33] These grain boundaries have proven to be low dissipative[5,6,34] compared to [001]-tilt ones and suitable for applications in quantum circuitry. By increasing the GB angle $\theta$, the interface gradually evolves into a 45° [010] twist GB at $\theta = 90^\circ$ (see Fig. 4).

### A. Noise properties of soft-patterned junctions

In Fig. 5(a), the voltage noise spectral density at 10 Hz is plotted as a function of the bias current $I$ for one of our soft-patterned nanojunctions having a width $w \simeq 200$ nm and nominal interface angle of 30°. However, by examining the grain boundary by AFM, the actual interface angle was closer to 0°.

As expected, the noise peaks close to the critical current when $I \simeq I_C = 4$ $\mu$A. A second peak appears close to $I = 5.2$ $\mu$A. This is due to a resonance feature in the IVC causing the differential resistance ($R_d$) to spike. For higher bias, where the resistance fluctuations dominate, the noise increases quadratically. The hump structure around 50 $\mu$A

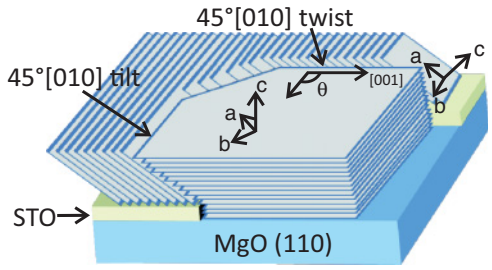


FIG. 4. (Color online) (a) Sketch of the interface geometry. The crystallographic orientations of the (001) and (103) YBCO are indicated by arrows. $\theta$ is the interface angle and is defined with respect to the [001] MgO direction.

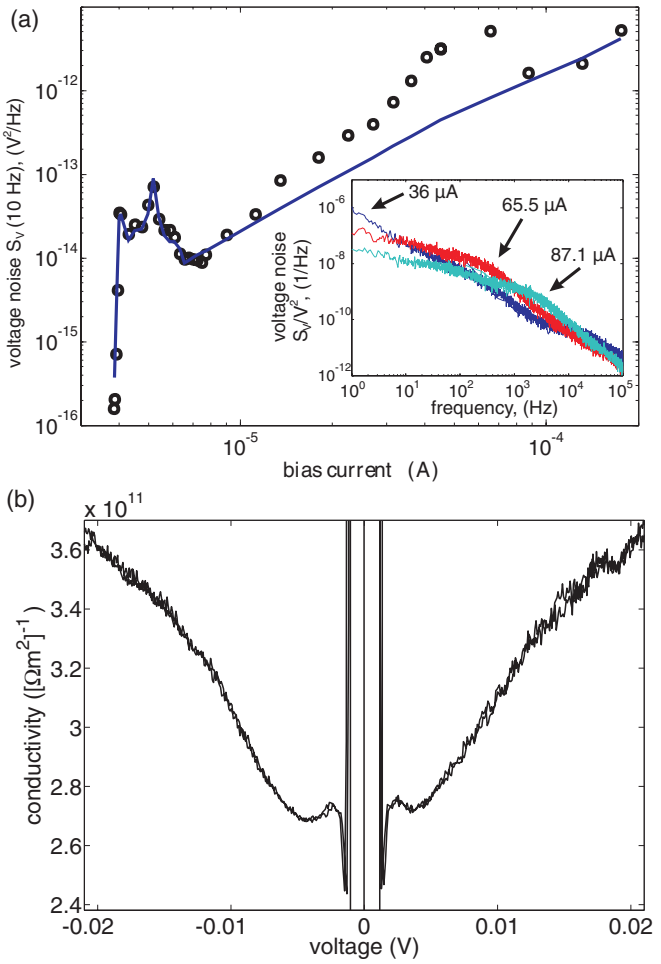


FIG. 5. (Color online) (a) Voltage noise at 10 Hz as a function of bias current (open symbols) for a soft-nanopatterned junction (the nominal interface angle is 30°). A theoretical fit (solid line) is included to determine $S_I$ and $S_R$. The inset shows the voltage noise as a function of frequency for three different bias points. The "hump" moves to higher frequencies when the bias is increased. (b) Conductivity as a function of bias voltage of the soft-nanopatterned junction. The central part ($|V| < 1$ mV) is related to the Josephson effect.

is caused by a single charge trap causing an RTS signal with a typical Lorentzian spectrum on top of a $1/f$ background. The occurrence of such Loretzians is typical for a limited number of charge traps in submicrometer-sized GB junctions.[15] The voltage dependence of the effective lifetime of the charge trap causes the Lorentzian to move to higher frequencies for increasing bias current, which is shown in the inset of Fig. 5.

To fit the measured voltage noise spectral density at 10 Hz as a function of bias current [see solid line in Fig. 5(a)] to Eq. (4), which assumes a pure $1/f$ noise spectrum, we neglected the data between 20 and 80 $\mu$A caused by a single charge trap. From the fit, we obtain $S_I \simeq S_R \simeq 10^{-8}$/Hz resulting in $q = |\delta I_C/I_C|/|\delta R_N/R_N| \simeq 1$ and $k \simeq -1.3$. The ratio $q \simeq 1$ indicates that our junction has a rather homogeneous barrier, where quasiparticles and Cooper pairs tunnel directly through the same parts of the barrier.[10] Together with a tunnel-like conductance spectrum [see Fig. 5(b)] we can conclude that our junction barrier is very similar to that of an SIS junction, consistent with the band-bending model.[35,36] Similar

TABLE I. Collection of 1/f noise in HTS GB Josephson junctions of different HTS materials, GB interface types, technology, and junction areas $A_j$. The interface angle $\theta$ of the soft-patterned junctions is illustrated in Fig. 4. The values $\alpha$ and $\beta$ are given by $\cos^2(2\pi\theta/360)$ and $\sin^2(2\pi\theta/360)$, respectively.

| Junction technology | GB type | $A_j$ ($\mu$m$^2$) | $S_I^{1/2}$ (10 Hz) $\times 10^{-4}$(Hz$^{-1/2}$) | $q = (S_I/S_R)^{1/2}$ | $A_j^{1/2} S_I^{1/2}$ (10 Hz) $\times 10^{-6}$($\mu$m/Hz$^{1/2}$) |
|---|---|---|---|---|---|
| YBCO/STO/MgO biepitaxial $\theta \simeq 0°$ (this work) | 45° [010] tilt | 0.02 | $1.0 \pm 0.1$ ($T = 4.2$ K) | $1.0 \pm 0.1$ | 14 |
| YBCO/STO/MgO biepitaxial $\theta \simeq 50°$ (this work) | $\alpha${45° [010] tilt}+ $\beta${45° [010] twist} | 0.052 | $1.6 \pm 0.1$ ($T = 4.2$ K) | $1.8 \pm 0.2$ | 36 |
| YBCO/$NdGaO_3$ bicrystal (Ref. 14) | $2 \times 14°$ [100] tilt | 0.06 | $0.36 \pm 0.06$ ($T = 55$ K) | $1.05 \pm 0.1$ | 10 |
| YBCO/STO bicrystal (Ref. 9) | 25° [001] tilt | 1.0 | 0.32 ($T = 70$ K) | 2.5 | 32 |
| $Bi_2Sr_2CaCu_2O_{8+x}$/STO bicrystal (Ref. 11) | 24° [001] tilt | 1.6 | $0.24 \pm 0.06$ ($T = 40$–$70$ K) | $1.9 \pm 0.3$ | 30 |
| YBCO/STO bicrystal (Refs. 12 and 13) | 24° [001] tilt | 3.8 | $0.18 \pm 0.01$ ($T = 25$–$70$ K) | $3.8 \pm 0.6$ | 35 |
| YBCO/STO bicrystal (Refs. 12 and 13) | 36.8° [001] tilt | 1.0 | $0.35 \pm 0.12$ ($T = 30$–$70$ K) | $3.7 \pm 0.8$ | 35 |

results have only been found in $2 \times 14°$ [100]-tilt YBCO GB Josephson junctions.[14] Furthermore, our result is incompatible with the intrinsically shunted junction model[11,12,31,32] and the channel model,[10] where $q$ values larger than two are expected. The deviation of the correlation between the critical current and resistance fluctuations from perfect anticorrelation ($k = -2$) could be caused by the limited amount of two-level fluctuators in the small junction area not representing a perfect ensemble. It is important to point out that the noise properties of our nanojunction close to an ideal SIS Josephson junction underline once more the pristine character of the junction barrier that can be obtained by using the soft-nanopatterning method.

In Fig. 6, the voltage noise spectral density at 10 Hz is plotted for a 520-nm-wide sample having a nominal

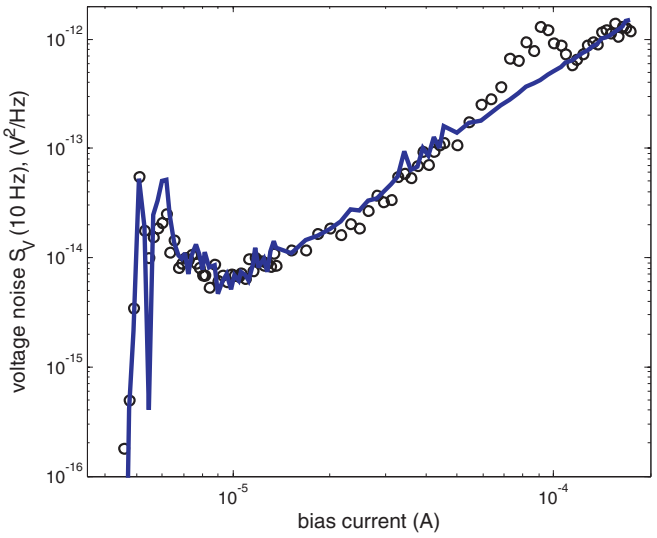


FIG. 6. (Color online) Voltage noise at 10 Hz as a function of bias current (open symbols) of a soft-nanopatterned junction with an interface angle of 50°. The solid line is a theoretical fit used to determine $S_I$ and $S_R$.

interface angle of $\theta \simeq 50°$. This value was confirmed by the AFM inspection of the GB. From the fit we obtain $S_I \simeq 2 \times 10^{-8}$–$3 \times 10^{-8}$/Hz, $S_R \simeq 8 \times 10^{-9}$/Hz, and $k \simeq -0.5$ resulting in $q = 1.8 \pm 0.2$. The $q$ value close to two indicates that the transport across the GB barrier cannot be described by a direct tunneling model, e.g., a homogeneous SIS tunnel junction. Instead, our result shows that for this kind of GB type (mixture of 45°-[010] twist and 45°-[010] tilt) the barrier is better described by the ISJ model, where quasiparticles tunnel resonantly via localized states.

In Table I, we summarize the noise data of the soft nanopatterned biepitaxial YBCO GB junctions together with results from literature on HTS Josephson junctions of various GB types. Comparing the ratios $q = (S_I/S_R)^{1/2}$ between different GB types, one can clearly see that only GBs where the *ab* planes in at least one of the electrodes are tilted around an axis parallel to the GB interface, e.g., 45°-[010] tilt (this work) and $2 \times 14°$-[100] tilt,[14] have a ratio $q \simeq 1$. All the other GB types such as [001] tilt[9,11–13] and $\alpha${45° [010] tilt} + $\beta${45° [010] twist}, with $0 < \beta \leqslant 1$ exhibit ratios $q \gtrsim 2$. These facts give a strong indication that the nature of HTS GB barriers depends on how the *ab* planes meet at the interface. GBs with *ab* planes tilted around an axis parallel to the GB interface, such as a basal plane GB, can be described by a direct tunneling model consistent with a homogeneous SIS barrier. All other GB types deviating from a bare rotation of the *ab* planes around the GB line are characterized by resonant quasiparticle tunneling via localized states (ISJ model).

From the spectral density of the critical current fluctuations and the junction area, one can obtain information about the areal charge trap density $n_t$ and the cross-sectional area $A_t$ of the charge traps.[39,40] Assuming $N$ identical and independent charge traps, the spectral density of the relative critical current fluctuations scales with the junction area $A_j$ as $\langle(\delta I_C/I_C)^2\rangle = N(A_t/A_j)^2 = n_t A_t^2/A_j$. From this equation, it follows that the quantity $(S_I A_j)^{1/2}$ is proportional to the product of cross-sectional area of a charge trap and the square root of the trap

density $A_t n_t^{1/2}$. In Table I, we show the computed product $(S_I A_j)^{1/2}$ at 10 Hz for the various GB types. Remarkably, the values for GBs having ratios $q \geqslant 2$ are close to $35 \times 10^{-6}$ $\mu$m/Hz$^{1/2}$.[41] Instead, the values for $(S_I A_j)^{1/2}$ in GB types with $q \simeq 1$ are roughly three times smaller. Assuming that the cross-sectional area of a charge trap is independent of the GB type, the difference in charge trap density supports once more the different nature of the GB barriers.

In the following, we will use the Lorentzian spectra sitting on top of a $1/f$ background (see inset of Fig. 5) to estimate the cross-sectional area $A_t$ of a single charge trap in the barrier: a single charge trap causes the voltage across the junction to fluctuate between two bistable states with an amplitude $\Delta V$ (see inset in Fig. 7). For large bias currents $I \gg I_C$, when the differential resistance is asymptotically reaching the normal state resistance of the junction, we can write for the respective relative resistance change $\Delta R_N/R_N = \Delta V/V$. Assuming that the current flow across the junction is homogeneous and the charge trap completely blocks the current flow in a small part of the junction barrier, we can determine the charge trap's cross-sectional area $A_t$ from the measured voltage fluctuation amplitude $\Delta V$:

$$A_t = \frac{\Delta R_N}{R_N} A_{\rm qp} = \frac{\Delta V}{V} A_{\rm qp}, \tag{5}$$

where $A_{\rm qp}$ is the total area of quasiparticle transport along the junction. Instead of extracting $\Delta V$ from a voltage time trace, one can also use the mean-squared fluctuation amplitude $\langle(\delta V)^2\rangle$ determined from a Lorentzian fit of the noise spectrum (see Fig. 7). The two quantities are related via[15]

$$(\Delta V)^2 = \left(\frac{\tau_1}{\tau_2} + \frac{\tau_2}{\tau_1} + 2\right) \langle(\delta V)^2\rangle. \tag{6}$$

For clearly visible Lorentzians in the measured noise spectra, the ratio between the two mean lifetimes is typically in the range from 1 to 10. Hence, we can approximate the fluctuation amplitude within a factor of two by $\Delta V \simeq 2\sqrt{\langle(\delta V)^2\rangle}$ using the root mean-squared (rms) fluctuation amplitude extracted from a Lorentzian spectrum (see Fig. 7):

$$S_V^{\rm RTS}(f) = V^2 S_R^{\rm RTS}(f). \tag{7}$$

Together with Eq. (3), we can extract $\delta R_N/R_N$ and approximate the cross-sectional area of a charge trap:

$$A_t \simeq 2\frac{\delta R_N}{R_N} A_{\rm qp}. \tag{8}$$

From the results of the previous section, we can make the following considerations: (1) the $I_C$ versus $B$ measurements have shown that the modulation period corresponds to an effective width close to the nominal width of the junctions. We can therefore assume that the Cooper-pair transport is along the whole grain boundary, $A_{\rm cp} \simeq A_j$. (2) The fitting of the voltage noise spectral density has shown that $S_I \simeq S_R$, this tells us that the area of the superconducting channel is approximately equal to the quasiparticle one, $A_{\rm cp} \simeq A_{\rm qp}$. These two facts imply that the areas of both transport channels are very close to the nominal junction area ($A_{\rm qp} \simeq A_{\rm cp} \simeq A_j$). One can, therefore, use the nominal area, measured by AFM or SEM, in combination with the noise measurement to extract $A_t$. Here, we also use the fact that the junction thickness is approximately equal to the film thickness (120 nm). We have made this type of analysis for three soft-patterned junctions and fitted a total of 24 Lorentzians in the high-bias range on different spectra. The extracted distribution of $A_t$ is plotted in Fig. 8; we get an average area for the fluctuators of about 72 nm$^2$, which is comparable to results found in submicrometer [001]-tilt YBCO GB junctions.[15]

In Fig. 9, the spectrum at a bias current close to $I_C$ has been fitted by two Lorentzians and a weak $1/f$ background.

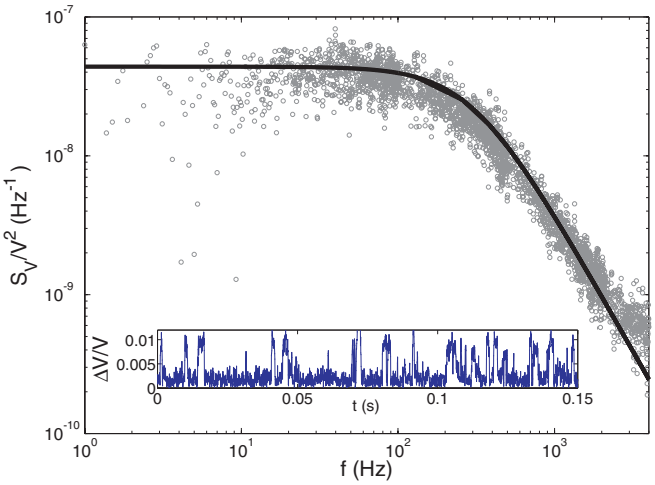


FIG. 7. (Color online) Noise spectrum measured at $I \gg I_C$ after the subtraction of the $1/f$ background. The black line is a Lorentzian fit to Eq. (7). The plateau of the Lorentzian is given by $4\tau_{\rm eff}\langle(\delta V/V)^2\rangle$, with $2\pi\tau_{\rm eff} = 302$ Hz and $\delta V/V = 0.0044$. The inset shows the respective time trace with $\Delta V/V \simeq 0.0095$.

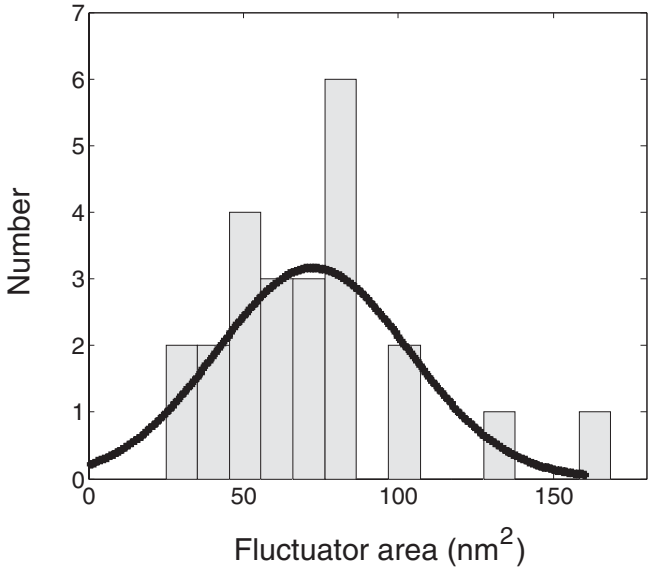


FIG. 8. Histogram showing the effective fluctuator area that was extracted from multiple spectra of three different soft-patterned junctions in the high-bias range. The black curve is a normal distribution with the same mean and standard deviation as the data set.

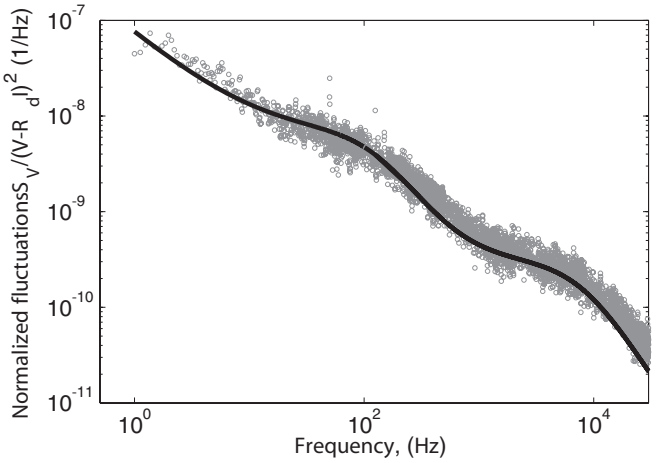


FIG. 9. Noise spectrum (open circles) and fit of two Lorentzians with a $1/f$ background (solid line) for one of the soft-nanostructured junctions measured at $I \simeq I_C$.

Since the contribution from $R_N$ fluctuations is negligible for this range of currents one can extract $\delta I_C/I_C$ using Eq. (3) and

$$S_I^{\mathrm{RTS}}(f) = \frac{S_V^{\mathrm{RTS}}(f)}{(V - R_d I)^2}. \tag{9}$$

The extracted values for $\delta I_C/I_C$ and $\delta R_N/R_N$ are fairly similar in magnitude, $\delta I_C/I_C$ being at most three times larger than the average of $\delta R_N/R_N$. This difference could be explained by a spread in the fluctuators area. Indeed, the values of $\delta I_C/I_C$ extracted close to $I_C$ will certainly come from different two-level fluctuators than those generating $\delta R_N/R_N$ fluctuations at high biases.

### B. Noise properties of conventional junctions

Identical measurements and analysis were carried out for three nanosized junctions fabricated by conventional nanolithography. For these samples, at bias currents slightly above $I_C$, we have observed the presence of strong Lorentzians in the low-frequency spectra caused by single charge traps, see Fig. 10(a). This circumstance makes the fitting of the data to Eq. (4) in the low-bias range impossible, therefore preventing the extraction of $S_I$ and the comparison with $S_R$. However, for these junctions, we were able to fit the Lorentzian voltage noise spectra for the two different bias ranges, where they are dominated by current fluctuations (close to $I_C$), $S_I^{\mathrm{RTS}}$, and by resistance fluctuations (far above $I_C$), $S_R^{\mathrm{RTS}}$, respectively, see Fig. 10. Assuming that the average effective area of the charge traps is roughly the same as that extracted from the junctions fabricated by soft nanopatterning, we can estimate $A_{\mathrm{cp}}$ and $A_{\mathrm{qp}}$ for the conventionally fabricated junctions.[42] The part of the junction area manifesting Josephson coupling and quasiparticle transport can be approximated by $A_{\mathrm{cp}} \simeq A_t I_C/2\delta I_C$ and $A_{\mathrm{qp}} \simeq A_t R_N/2\delta R_N$, respectively. In the insets of Fig. 10, we show the spectral density of the normalized fluctuations multiplied by the frequency. The pronounced difference between the fluctuation amplitudes of the Lorentzians in the critical current and resistance noise spectra by several orders of magnitude clearly manifests the difference in area for the quasiparticle and Cooper-pair transport channels. In

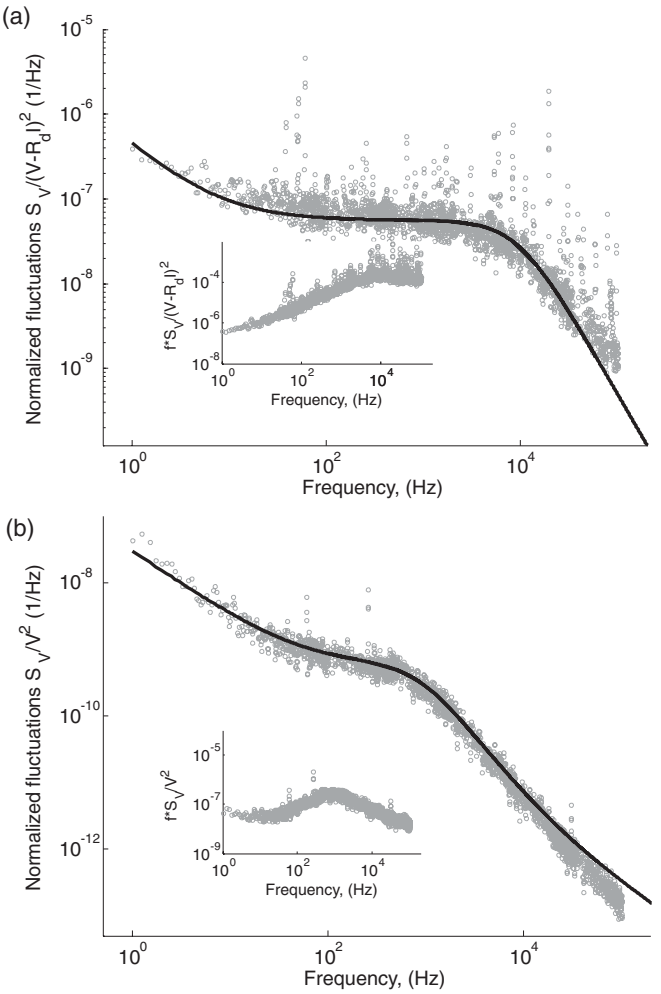


FIG. 10. Noise spectrum (open circles) and fit of a Lorentzian with a $1/f$ background (solid line) for a conventionally patterned junction measured at (a) $I \simeq I_C$ and (b) $I \gg I_C$. The vertical axis show the normalized fluctuations corresponding to (a) $S_I$ and (b) $S_R$. The insets shows normalized fluctuations multiplied by the frequency to emphasize the amplitude of the charge traps.

Table II, we summarize the results for three conventionally patterned junctions. The average quasiparticle area is 25–50% less than the nominal area. However, the superconducting area varies greatly and for two of the junctions it is significantly less than the quasiparticle area. The $A_{\mathrm{qp}}$ extracted from the noise measurements tells us that the grain boundaries, despite losing most of the Josephson properties, still have a quasiparticle transport channel with an average area comparable to the

TABLE II. Total nominal area $A_j$, area for the quasiparticle transport channels $A_{\mathrm{qp}}$, and area for superconducting transport channels $A_{\mathrm{cp}}$ (extracted from noise data) for three conventionally patterned samples.

| Junction number | $A_j$ (nm$^2$) | $A_{\mathrm{qp}}$ (nm$^2$) | $A_{\mathrm{cp}}$ (nm$^2$) |
|---|---|---|---|
| 1 | 50 000 | 31 500 | 1250 |
| 2 | 30 000 | 14 600 | 9060 |
| 3 | 30 000 | 22 300 | 160 |

nominal area. The area of the quasiparticle channel does not decrease much in the fabrication process for the conventional junctions, however the resistivity of the channel seem to increase. Evaluating the critical current density based on the effective area across which Cooper-pair transport occurs results in $j_C^{\text{eff}} = I_C/A_{\text{cp}} \simeq 2$–$20$ kA/cm$^2$, where $I_C$ is the critical current of the conventionally patterned junctions. Here, it is interesting to note that these values are in the same range as those found in pristine soft-nanostructured GB junctions.[16] This fact clearly reflects the strong dependence of the Josephson coupling on the stoichiometry in close proximity (length scale of coherence length) of the GB. The detrimental effect of the ion etching process during the conventional nanopatterning seems to locally kill the Josephson coupling rather than inducing a gradual decrease over the whole junction area. The ion beam procedure appears to be an on-off process for the Josephson coupling; the grain boundary region that survives the ion bombardment preserves the same Josephson properties as the untouched soft-nanopatterned samples. The overall increase of more than one order of magnitude of the GB resistivity of conventionally fabricated nanojunctions compared to the soft-nanopatterned ones can therefore be related to a reduced barrier transparency in the junction regions where the Josephson coupling has been switched off in the milling procedure.

## VI. SUMMARY AND CONCLUSIONS

To summarize, we have compared the electrical transport and noise properties for nanoscaled biepitaxial YBCO grain-boundary Josephson junctions fabricated by two different methods. From electrical transport and $1/f$ voltage noise properties of soft-nanopatterned Josephson junctions with a GB characterized by a rotation of the $ab$ planes parallel to the interface (large $c$-axis tunneling component), we can conclude that the GB barrier is very homogeneous and has a SIS character (direct tunneling model). Instead, the noise properties of soft-patterned junctions, where the transport is dominated by tunneling parallel to the $ab$ planes, are in accordance with a resonant tunneling model (ISJ model). From the analysis of two-level fluctuators in the barrier, on the other hand, we find that the conventional nanofabrication method severely deteriorates the Josephson properties of the GB. The junction area maintaining Josephson current can on average be much smaller than the nominal area, while the quasiparticle transport area is similar to the nominal one. In this case, the transport across the GB interface can be well described by the transport model proposed by Miklich.[10] The resistivity in these samples is increased compared to the soft-nanopatterned GB junctions. The noise properties of our nanojunctions allow to identify two classes of experiments that one can perform by taking advantage of the specifics of the transport properties: (1) to realize quantum bits by employing soft nanopatterned junctions (the pristine grain boundary is an ideal candidate to study the intrinsic source of dissipation in HTS by measuring relaxation and coherence times in a quantum bit) and (2) to realize devices where charging effects are dominant. The large resistivity values of the conventionally patterned junctions $\rho_N \simeq 5 \times 10^{-7}$–$2 \times 10^{-6}$ $\Omega$cm$^2$ make these junctions good candidates for the realization of all-HTS single-electron transistors, which can be used to study possible subdominant order parameters in HTS materials.[43]

## ACKNOWLEDGMENTS

This work has been partially supported by EU STREP project MIDAS, the Swedish Research Council (VR) under the Linnaeus Center on Engineered Quantum Systems, the Swedish Research Council (VR) under the project Fundamental properties of HTS studied by the quantum dynamics of two-level systems, and the Knut and Alice Wallenberg Foundation.

*dagust@chalmers.se

[1] D. Koelle, R. Kleiner, F. Ludwig, E. Dantsker, and J. Clarke, Rev. Mod. Phys. **71**, 631 (1999).
[2] L. Alff, A. Beck, R. Gross, A. Marx, S. Kleefisch, T. Bauch, H. Sato, M. Naito, and G. Koren, Phys. Rev. B **58**, 11197 (1998).
[3] C. C. Tsuei and J. R. Kirtley, Rev. Mod. Phys. **72**, 969 (2000).
[4] J. Johansson, K. Cedergren, T. Bauch, and F. Lombardi, Phys. Rev. B **79**, 214513 (2009).
[5] T. Bauch, F. Lombardi, F. Tafuri, A. Barone, G. Rotoli, P. Delsing, and T. Claeson, Phys. Rev. Lett. **94**, 087003 (2005).
[6] T. Bauch, T. Lindström, F. Tafuri, G. Rotoli, P. Delsing, T. Claeson, and F. Lombardi, Science **311**, 57 (2006).
[7] T. Bauch, D. Gustafsson, K. Cedergren, S. Nawaz, M. Mumtaz Virk, H. Pettersson, E. Olsson, and F. Lombardi, Phys. Scr. T **173**, 014006 (2009).
[8] D. Gustafsson, T. Bauch, S. Nawaz, M. Mumtaz Virk, G. Signorello, and F. Lombardi, Physica C **470**, S188 (2010).
[9] M. Kawasaki, P. Chaudhari, and A. Gupta, Phys. Rev. Lett. **68**, 1065 (1992).
[10] A. H. Miklich, J. Clarke, M. S. Colclough, and K. Char, Appl. Phys. Lett. **60**, 1899 (1992).
[11] A. Marx, U. Fath, W. Ludwig, R. Gross, and T. Amrein, Phys. Rev. B **51**, 6735 (1995).
[12] A. Marx, U. Fath, L. Alff, and R. Gross, Appl. Phys. Lett. **67**, 1929 (1995).
[13] A. Marx, L. Alff, and R. Gross, Appl. Supercond. **6**, 621 (1998).
[14] M. V. Liatti, U. Poppe, and Y. Y. Divin, Appl. Phys. Lett. **88**, 152504 (2006).
[15] F. Herbstritt, T. Kemen, L. Alff, A. Marx, and R. Gross, Appl. Phys. Lett. **78**, 955 (2001).
[16] D. Gustafsson, H. Pettersson, B. Iandolo, E. Olsson, T. Bauch, and F. Lombardi, Nano Lett. **10**, 4824 (2010).
[17] P. V. Komissinski, B. Högberg, A. Y. Tzalenchuk, and Z. Ivanov, Appl. Phys. Lett. **80**, 1022 (2002).
[18] T. Lindström, J. Johansson, T. Bauch, E. Stepantsov, F. Lombardi, and S. A. Charlebois, Phys. Rev. B **74**, 014503 (2006).
[19] D. Stornaiuolo, G. Rotoli, K. Cedergren, D. Born, T. Bauch, F. Lombardi, and F. Tafuri, J. Appl. Phys. **107**, 113901 (2010).

[20]D. Stornaiuolo, K. Cedergren, D. Born, T. Bauch, A. Barone, F. Lombardi, and F. Tafuri, IEEE Trans. Appl. Supercond. **19**, 174 (2009).
[21]U. Scotti di Uccio, F. Miletto Granozio, A. Di Chiara, F. Tafuri, O. I. Lebedev, K. Verbist, and G. van Tendeloo, Physica C **321**, 162 (1999).
[22]A. Di Chiara *et al.*, Physica C **273**, 30 (1996).
[23]M. Tinkham, *Introduction to Superconductivity*, 2nd ed. (Dover, New York, 2004).
[24]K. Likharev, *Dynamics of Josephson Junctions and Circuits*, 1st ed. (Gordon and Breach Science, New York, 1986).
[25]P. A. Rosenthal, M. R. Beasley, K. Char, M. S. Colclough, and G. Zaharchuk, Appl. Phys. Lett. **59**, 2482 (1991).
[26]The two formulas for $\Delta B$ are valid in the short junction limit, $w_j < 4\lambda_j$,[24] where $\lambda_j$ is the Josephson penetration depth,[27] $\lambda_j^2 = \hbar/[2ej_C\mu_0(\lambda_{001} + \lambda_{103} + d)]$. For the soft-nanopatterned junctions, we get $\lambda_j \simeq 1.2$ $\mu$m. All measured junctions are in the short-junction limit since $w_j < 4\lambda_j$.
[27]T. Van Duzer and C. W. Turner, *Superconductive Devices and Circuits*, 2nd ed. (Prentice Hall, New Jersey, 1999).
[28]$\lambda_{ab}$ for a critical temperature ($T_c$) of 89 K is approximately 160 nm.[38] The effective London penetration depth, $\lambda_{\text{eff}}$, was obtained using $\lambda_c = 2$ $\mu$m (Ref. 37) and geometrical considerations[4] with a dependence on the grain boundary angle.
[29]C. T. Rogers and R. A. Buhrman, Phys. Rev. Lett. **53**, 1272 (1984).
[30]S. Machlup, J. Appl. Phys. **24**, 341 (1954).
[31]R. Gross, L. Alff, A. Beck, O. M. Froehlich, D. Koelle, and A. Marx, IEEE Trans. Appl. Supercond. **7**, 2929 (1997).
[32]R. Gross, P. Chaudhari, M. Kawasaki, and A. Gupta, Phys. Rev. B **42**, 10735 (1990).
[33]K. Cedergren, H. Pettersson, E. Olsson, T. Bauch, and F. Lombardi (unpublished).
[34]F. Lombardi *et al.*, Physica C **435**, 8 (2006).
[35]J. Mannhart and H. Hilgenkamp, Mater. Sci. Eng. B **56**, 77 (1998).
[36]H. Hilgenkamp and J. Mannhart, Appl. Phys. Lett. **73**, 265 (1998).
[37]C. C. Homes, S. V. Dordevic, D. A. Bonn, Ruixing Liang, W. N. Hardy, and T. Timusk, Phys. Rev. B **71**, 184515 (2005).
[38]Y. Zuev, M. S. Kim, and T. R. Lemberger, Phys. Rev. Lett. **95**, 137002 (2005).
[39]A. Marx and R. Gross, Appl. Phys. Lett. **70**, 120 (1997).
[40]D. J. van Harlingen, T. L. Robertson, B. L. T. Plourde, P. A. Reichardt, T. A. Crane, and J. Clarke, Phys. Rev. B **70**, 064517 (2004).
[41]The constant value $(S_I A_j)^{1/2}$ is equivalent to the scaling behavior of the resistance fluctuations $S_R \propto R_N$ reported by Marx *et al.*[39]
[42]The $I_C$ versus $B$ pattern of the conventional junctions does not follow a Fraunhofer-like pattern. This hints that the interfaces consist of an array of superconducting channels. However, as long as the individual channels have an area greater than the effective area of the defects, Eq. (8) is still valid.
[43]S. E. Kubatkin, A. Ya. Tzalenchuk, Z. G. Ivanov, P. Delsing, R. I. Shekhter, and T. Claeson, JETP Lett. **63**, 126 (1996).